CHEMICAL ENGINEERING TRANSACTIONS
VOL. 120, 2025
A publication of AIDIC
The Italian Association of Chemical Engineering
Online at www.cetjournal.it
Guest Editors: Bing Shen How, Viknesh Andiappan, Denny K.S. Ng, Hon Loong Lam, Petar S. Varbanov

ISBN 979-12-81206-21-2; **ISSN** 2283-9216
DOI: 10.3303/CET25120030

Soft-sensor Modeling of Vessel Interior Temperatures under Different Nozzle Configurations in a Cooling Process

Jinxin Wang[a], Feng Xu[a], Yuka Sakai[a], Hisashi Takahashi[b], Ruizi Zhang[c], Hiroaki Kanayama[c], Daisuke Satou[c], Yasuki Kansha[a,*]

[a]Organization for Programs on Environmental Sciences, Graduate School of Arts and Sciences, The University of Tokyo, 3-8-1 Komaba, Meguro-ku, Tokyo 153-8902, Japan
[b]TechnoPro, Inc. TechnoPro R&D Company, Roppongi Hills Mori Tower 35F, 6-10-1 Roppongi, Minato-ku, Tokyo 106-6135, Japan
[c]Technology and Innovation Center, Daikin Industries, LTD., 1-1 Nishi-Hitotsuya, Settsu, Osaka 566-8585, Japan
kansha@global.c.u-tokyo.ac.jp

Temperature monitoring plays an important role in industrial processes, and soft sensors have attracted increasing attention for this purpose. This study evaluates the performance of a gray-box soft sensor model, which requires only online temperature data at the nozzle and at one reference location as inputs, for vessel interior temperature prediction in a cooling process with different jet inflows. Lab-scale experiments of water vessels were conducted with two types of nozzles to measure local temperatures at multiple locations. The model was trained by a data set, and validated by another data set under the same conditions except for nozzle types. The reference location selection was found to be able to significantly influence the model's predictive accuracy. Flow visualization experiments were performed to analyze fluid dynamics near the reference location. Significant flow-pattern variations were found in its vicinity, which may affect predictive accuracy. Results show that the model can achieve satisfactory error levels under varied flow fields induced by different nozzle configurations, with mean and maximum errors reduced to below 0.5 °C and 1.1 °C, respectively. The findings highlight the unfavorable influences of inflow-induced convection on predictive performance and demonstrate that appropriate reference selection plays an important role in predictive accuracy. This study widens the applicable scenarios of a gray-box soft sensor in industrial thermal processes and related fields, such as air conditioning.

1. Introduction

Temperature monitoring is crucial for ensuring product quality, energy efficiency, and safe operation in industrial processes. However, installing physical sensors at critical locations within process vessels is often impractical due to harsh environments, space limitations, and high costs. To overcome these limitations, soft sensors (or virtual sensors) have attracted increasing attention (Jiang et al., 2021). As inferential models, they enable the estimation of hard-to-measure variables based on easily accessible measurements (Mei et al., 2023). For fluid temperature predictions, soft sensors have shown promise in applications such as tank filling (Bourgeois et al., 2015) and chemical reactors (Savarese et al., 2024), with examples also found in HVAC (heating, ventilation and air conditioning) systems (Mattera et al., 2018).

Current soft-sensor models for fluid temperature predictions are often tailored to specific conditions, which may overlook the influence of fluid dynamics (Xu et al., 2025). However, some flow-supplying conditions, like jet orientation, can significantly alter internal flow fields in a vessel, affecting mixing efficiency (Oluwadero et al., 2023). Additionally, nozzle dimensions have also been reported to affect mixing time (Patwardhan and Gaikwad, 2003). Therefore, it can be challenging for a soft-sensor model to maintain accuracy under varied flow fields induced by different nozzle configurations, which limits its applicable scenarios.

To address this issue, this study examined a gray-box soft sensor model using two differently configured nozzles in a cooling process. The model requires only temperature information at the supply nozzle and at a reference

Paper Received: 15 May 2025; Revised: 2 September 2025; Accepted: 3 October 2025
Please cite this article as: Wang J., Xu F., Sakai Y., Takahashi H., Zhang R., Kanayama H., Satou D., Kansha Y., 2025, Soft-sensor Modeling of Vessel Interior Temperatures under Different Nozzle Configurations in a Cooling Process, Chemical Engineering Transactions, 120, 175-180 DOI:10.3303/CET25120030

location (Xu et al., 2023). Temperature data for modeling were obtained from measurements in a vessel. Flow visualization using Particle Image Velocimetry (PIV) was also conducted to analyze the differences in flow patterns and their influences near the reference location, which eventually may affect soft sensor accuracy. The discovered importance of reference location selection concerning the fluid dynamics will facilitate the applications of this soft-sensor model in industrial processes.

2. Methodology

2.1 Experimental setup

Temperature data from water-based experiments were collected, which were utilized for calculating model coefficients in training and predictive errors in validation (described in section 2.2). Figure 1a illustrates the water circulation system used in this investigation. Although Figure 1a specifically shows the setup for PIV experiments, the configuration used for temperature data collection was similar. During temperature data collection, the syringe pump (⑨) was inactive and the drain nozzle (⑧) was directly connected to the aspirator (⑪) without the trace filter (⑩). Therefore, the temperature measurement setup is not redundantly illustrated here. Further operational details of the system can be found in (Xu et al., 2023).

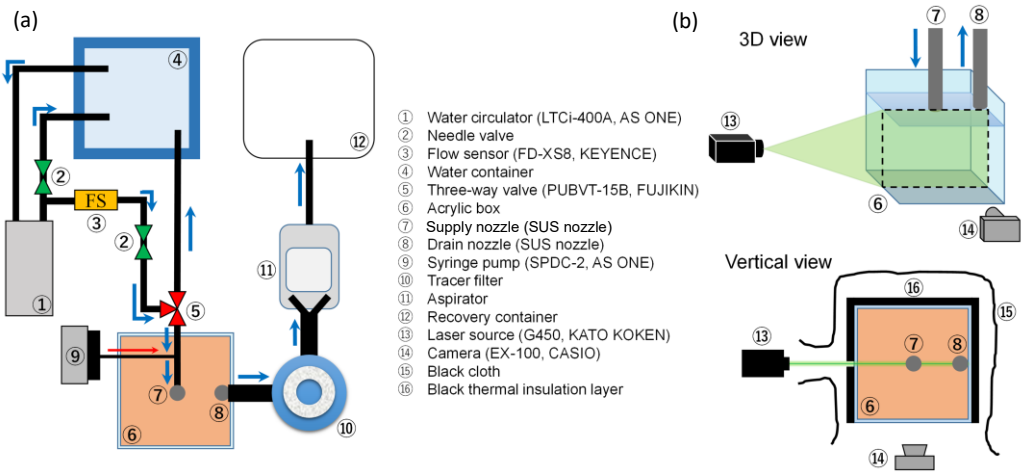

Figure 1: Schematic of experimental apparatus of water circulation system and PIV (adapted from (Xu et al., 2023) under CC BY license).

A cooling process in a vessel was simulated with this setup. The acrylic box (⑥) was initially filled with water at 35 °C, and cooling water at 10 °C was supplied through the supply nozzle (⑦). To assess the accuracy of the soft sensor model under varied flow patterns, two differently configured supply nozzles were employed. As shown in Figure 2a, the nozzles differed in inflow angle, geometry, and radius, and are hereafter referred to as the I-shaped and Y-shaped nozzles, respectively. In a recent study, the soft sensor model exhibited satisfactory prediction accuracy using the I-shaped nozzle across a wide range of conditions (Xu et al., 2025). In the present study, the model is also evaluated using the Y-shaped nozzle.

Thermocouples were installed both inside the vessel and within the supply nozzle to record temperatures at various locations, as indicated by black dots in Figures 2b and 2c. The thermocouples were arranged across three horizontal layers (Figure 2b), following the naming convention used in earlier literature (Xu et al., 2023). In this study, the middle layer was selected for investigation. B1M, B2M, and D2M, as shown in Figure 2c, represent typical interior locations within the vessel and were selected as the target sites for temperature prediction. Temperature data were recorded for 900 s from the start of the water supply, with a sampling interval of 0.1 s. The temperature data collected from all measurement locations in one experiment formed a data set. In total, four data sets were used in this study for modeling purposes.

As summarized in Table 1, for each nozzle case, the experiment was repeated once under identical experimental conditions to allow the model training and validation to be performed separately with two independent data sets. Specifically, model training employed data set i1L1 and data set y1, which were then validated with data set y1 and data set y2, respectively. Data set i1 was obtained from the work of Xu et al. (2023) to conserve experimental resources, while the other three were newly conducted for this study.

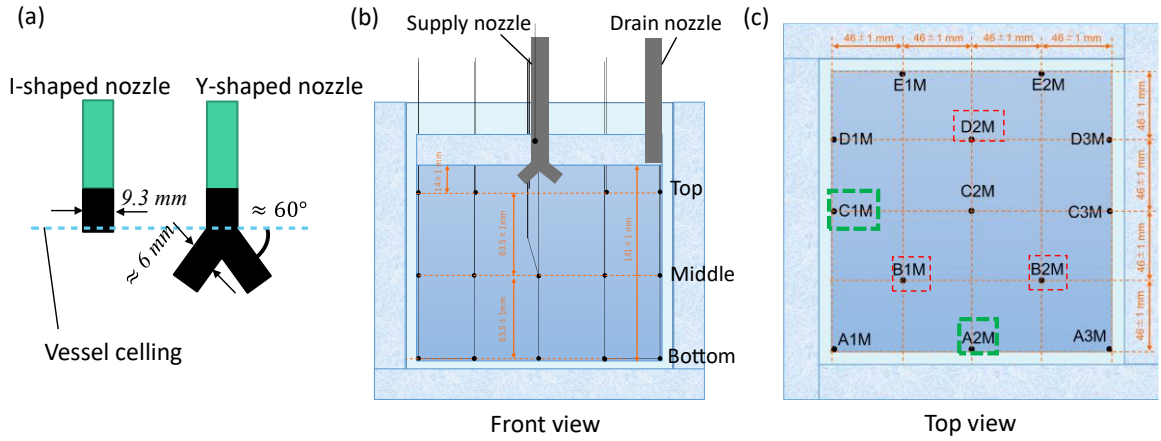

Figure 2: (a) two nozzles of different configurations; (b) the layout of thermocouples in the front view; (c) the layout of thermocouples in the middle layer with reference location candidates (green) and interior target sites (red) marked.

Table 1: Temperature data set information.

Data set name	i1	i2	y1	y2
Nozzle type	I shape	I shape	Y shape	Y shape
Initial temperature [°C]	35	35	35	35
Supply temperature [°C]	10	10	10	10
Flow rate (mL/min)	770	770	770	770

2.2 Modeling method and error metrics

The soft sensor model was first developed by Xu et al. (2023), as shown in Eq(1). In this study, the model coefficients $(\alpha, \beta, \gamma, \delta)$ were obtained by solving the optimization problem defined in Eq(2), following the methodology adopted in the recent work by Xu et al. (2025). This approach incorporates physical constraints $(\beta + \gamma = 1, \beta > 0, \gamma > 0)$ which have been shown to significantly improve prediction accuracy. T_Y and $\hat{T}_Y$ denote the measured and predicted temperature at a target site (outlined in red in Figure 2c), respectively. T_S is the measured supply temperature, which oscillated around 10 °C within a range of ±0.5 °C. T_X represents the real-time temperature retrieved at a designated location used as the "reference data" input to the model. Accordingly, the location providing T_X is referred to as the "reference location" hereafter. Subscript $\boldsymbol{i}$ denotes the $\boldsymbol{i}$-th data point, for example, $T_{Y,i}$ denotes the $\boldsymbol{i}$-th measured temperature at a target site.

$$\hat{T}_Y = \alpha + \beta T_X + \gamma T_S + \delta \frac{dT_X}{dt} \tag{1}$$

$$\min\ f(\alpha, \beta, \gamma, \delta) = \sum_{i=1}^{9001} \left(T_{Y,i} - \alpha - \beta T_{X,i} - \gamma T_{S,i} - \delta \frac{dT_{X,i}}{dt}\right)^2$$
$$\text{s.t. } \beta + \gamma = 1, \beta > 0, \gamma > 0 \tag{2}$$

It should be noted that the reference location providing T_X is fixed during model training, whereas different target sites result in different sets of coefficients $(\alpha, \beta, \gamma, \delta)$ according to Eq(2). Therefore, each target site has its specific soft sensor model, which is herein referred to as a sub-model. In this study, two candidates were explored as the reference location: C1M and A2M, as outlined in green in Figure 2c.

To evaluate the model's prediction accuracy, three metrics were employed: mean absolute error (*MAE*), coefficient of determination (R^2), and maximum absolute error (*MaxAE*), as defined in Eq(4), Eq(5) and Eq(6), respectively. These metrics were calculated based on the discrepancy (ΔT_i) between measured and predicted values, as described in Eq(3). The *MaxAE* metric was newly introduced in this study to assess the severity of short-term prediction deviations, in addition to the *MAE* and R^2 used in prior work (Xu et al., 2025). In Eq(6), max denotes the maximum operator, and MA denotes the moving average operator, which uses a backward window of 10 s. Notably, the initial 40 s were excluded from the *MaxAE* calculation. Large T_S deviations (exceeding 1.5 °C) were measured from the target value (10 °C) in the initial 30 s due to limitations in the

experimental setup. As a result, unusually large errors $|\Delta\tilde{T}_i|$ were obtained in the period [10 s, 40 s] (10 s shift for the MA operation).

$$\Delta T_i = \hat{T}_{Y,i} - T_{Y,i} \tag{3}$$

$$MAE = (\sum_{i=1}^{9001} |\Delta T_i|)/n \tag{4}$$

$$R^2 = 1 - \frac{\sum_{i=1}^{9001} \Delta T_i^{\,2}}{\sum_{i=1}^{9001} (\hat{T}_{Y,i} - \overline{T_Y})^2} \tag{5}$$

$$MaxAE = \max_{401 \le i \le 9001} (|\mathrm{MA}(\Delta T_i)|) = \max_{401 \le i \le 9001} (|\Delta\tilde{T}_i|) \tag{6}$$

To differentiate specific data or sub-model validations, the following notation conventions are used:
(1) Local data is specified by postfixing data set name; for example, B1Mi1 refers to the temperature data at B1M in data set i1.
(2) Validation for a specific sub-model is denoted with combined data notations; for example, if a sub-model is trained using C1Mi1 and B1Mi1, its validation is denoted by C1Mi1-B1Mi2, representing the validation is against B1Mi2 (by referencing C1Mi2 certainly). For brevity, B1Mi1 and C1Mi2 are just omitted.

3. Results and discussions

3.1 Predictive accuracy at B1M

C1M and B1M were first chosen as the reference location and the target site, respectively, following previous studies with the I-shaped nozzle (Xu et al., 2023, 2025). It was found that the *MAE* for the Y-shaped nozzle case was 0.53 °C, which is higher than the 0.45 °C observed in the I-shaped nozzle case. Regarding *MaxAE*, the Y-shaped nozzle case (1.47 °C) was considerably more severe than the I-shaped case (1.00 °C), representing a 47 % increase. Figures 3a and 3b show the predicted versus measured temperatures as well as their discrepancies (defined in Eq(3)) for the two nozzle cases. Notably, C1My1-B1My2 exhibits larger ΔT values especially within the first 300 s, compared to those of C1Mi1-B1Mi2.

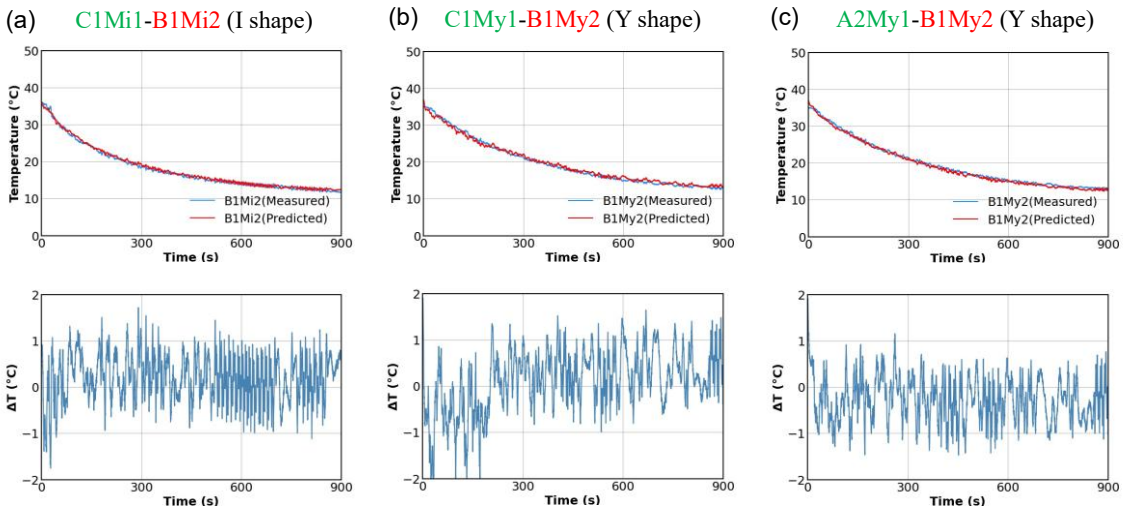

Figure 3: Measured vs. predicted temperatures at B1M in different cases (upper) and their corresponding discrepancies ΔT (lower).

A2M was explored as an alternative reference location. As Xu et al. (2025) reported that the flow patterns can affect the model accuracy (Figure 10), C1My1 and CiMy2 were suspected to be much more impacted by flows compared to C1Mi1 and C1Mi2. It is because C1M locates at the C1M-C2M-C3M line (Figure 2c), which is aligned with the bifurcations of the Y-shaped nozzle and thus can be more strongly suffered from flow variations concerning nozzle configurations. Therefore, A2M in the Y-shaped nozzle case became a considerable

alternative as the reference location, which not only locates at the wall center like C1M, but also should be less affected by flows induced from nozzle variations.
For A2My1-B1My2, the *MAE* is identical to C1Mi1-B1Mi2, i.e., 0.45 °C, while the *MaxAE* is marginally higher at 1.01 °C. As seen in Figures 3b versus 3c, the discrepancies were clearly mitigated throughout the period of 900 s.

3.2 Overall accuracy evaluation for vessel interior

To comprehensively evaluate the model's accuracy using A2M, sub-models for three interior target sites were trained both A2M and C1M as the reference location in the Y-shaped nozzle case. As summarized in Table 2, model details and metric results are grouped based on the reference data (C1Mi1, C1My1, and A2My1). From Table 2, overall declines in *MAE* and *MaxAE* can be observed when switching the reference data from C1My1 to A2My1. Red-marked numbers indicate the largest *MAE* and *MaxAE* values within each group, which can serve as the error level associated with specific reference data. Taking the error level of C1Mi1 as the baseline (*MAE*: 0.45 °C, *MaxAE*: 1.00 °C), the error level of C1My1 is higher by 24.4 % and 47.0 % for *MAE* and *MaxAE* (0.56 °C and 1.47 °C), respectively. By contrast, A2My1 exceeds the baseline by only 6.7 % and 6.0 % for *MAE* and *MaxAE*, and the absolute increases are minimal: +0.03 °C and +0.06 °C, respectively. Therefore, selection of the reference position significantly affects the model's prediction performance.
It is interesting that only the $\boldsymbol{\alpha}$ of C1My1 are all positive while the others are negative. $\boldsymbol{\alpha}$ represents the influence or error caused by other parameters, such as radiation (Xu et al., 2023), which serves as a correction role in this gray-box model. This means that selecting C1My1 (as T_X) resulted in the underestimation of T_Y. Moreover, $\boldsymbol{\beta}$ and $-\boldsymbol{\delta}$ ($-dT_X/dt$ and $-\boldsymbol{\delta}$ are positive) in C1My1 group are all smaller than those in the A2My1 group, whereas $\boldsymbol{\gamma}$ are all reversely higher. Therefore, it is noticeable that the reference location not only determines T_X itself, but can also affect the T_X's and T_S's influential weights on T_Y. Especially, when T_Y is underestimated, the T_S effect becomes stronger.

Table 2: Sub-model coefficients and validation results under different nozzle configurations.

Training reference	Targeted-site data	$\boldsymbol{\alpha}$	$\boldsymbol{\beta}$	$\boldsymbol{\gamma}$	$\boldsymbol{\delta}$	R^2	*MAE* [°C]	*MaxAE* [°C]
C1My1 (Y shape)	B1My2	0.208	0.912	0.088	-22.494	0.989	0.53	1.47
	B2My2	0.249	0.958	0.042	-14.598	0.989	0.56	1.38
	D2My2	0.382	0.949	0.051	-11.781	0.993	0.41	1.06
A2My1 (Y shape)	B1My2	-0.415	0.929	0.071	-28.205	0.992	0.45	1.01
	B2My2	-0.383	0.984	0.016	-16.125	0.996	0.32	0.83
	D2My2	-0.234	0.972	0.028	-13.936	0.991	0.48	1.06
C1Mi1 (I shape, for comparison)	B1Mi2	-0.279	0.911	0.089	-15.493	0.992	0.45	1.00
	B2Mi2	-0.327	0.899	0.101	-20.180	0.995	0.32	0.72
	D2Mi2	-0.110	0.952	0.048	-15.539	0.995	0.35	0.95

3.3 Flow field analysis

To investigate the reason for the above weight variations, flow fields for both nozzle cases were analyzed and compared using PIV. As shown in Figure 1b, the central region containing C1M was illuminated. Flow field results for both nozzle cases are presented in Figure 4 at 180 s and 600 s, with C1M marked. The flow patterns differ significantly between the two cases, particularly near C1M. In the I-shaped nozzle case, water impinges on the vessel bottom and then flows upward along the wall toward C1M. In contrast, in the Y-shaped nozzle case, the incoming water directly strikes the wall and rolls upward toward C1M. Therefore, in the I-shaped nozzle case, the flow is more likely to mix with residual water before reaching C1M, whereas in the Y-shaped case, less mixing may occur. Such differences in convection patterns are likely to cause distinct thermal correlations among the reference location (T_X), supply nozzle (T_S), and target site (T_Y). Consequently, C1M may no longer be suitable as the reference location under the Y-shaped nozzle condition. In summary, reference locations that are strongly influenced by forced convection from the supply nozzle should be avoided.

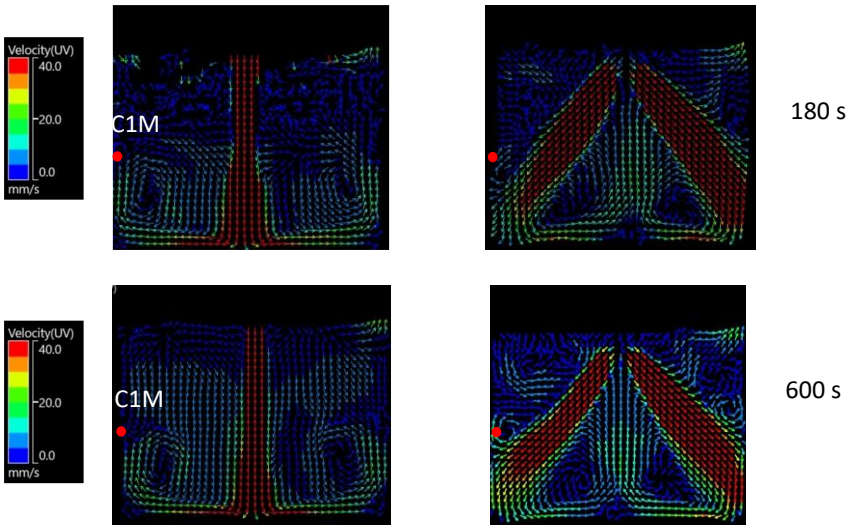

Figure 4: PIV results for different nozzle cases at 180 s (upper) and 600 s (lower)

4. Conclusions

In this study, a soft sensor model for predicting vessel interior temperature was evaluated using two different supply nozzles. The influences on modeling accuracy regarding the nozzle configurations were firstly investigated for this virtual sensor in a cooling process. Satisfactory accuracy ($MAE \leq 0.5$ °C; $MaxAE \leq 1.1$ °C) was ultimately maintained under varied inflow conditions. The key findings are summarized as follows:
(1) The soft sensor demonstrated accurate prediction performance in a cooling process despite significant changes in flow patterns caused by variations in nozzle configuration.
(2) The selection of the reference location, which the soft sensor model relies on, plays a critical role in predictive accuracy. It is advisable to choose a position that avoids strong forced convection from the supply nozzle.
This research contributes to the accurate temperature monitoring in industrial process, and it can also benefit the air-conditioning control system development.

Acknowledgments

This research is financially supported by New Energy and Industrial Technology Development Organization (NEDO), JPNP20004, Japan.

References

Bourgeois T., Ammouri F., Weber M., Knapik C., 2015, Evaluating the temperature inside a tank during a filling with highly-pressurized gas. International Journal of Hydrogen Energy, 40, 11748–11755.
Jiang Y., Yin S., Dong J., Kaynak O., 2021, A Review on Soft Sensors for Monitoring, Control, and Optimization of Industrial Processes. IEEE Sensors Journal, 21, 12868–12881.
Mattera C.G., Quevedo J., Escobet T., Shaker H.R., Jradi M., 2018, A Method for Fault Detection and Diagnostics in Ventilation Units Using Virtual Sensors. Sensors, 18, 3931.
Mei X., Kiyomoto H., Kato S., Kansha Y., 2023, Data-Driven Soft Sensor for Crude Oil Fouling Monitoring in Heat Exchanger Networks. IEEE Sensors Journal, 23, 26336–26346.
Oluwadero T.A., Xuereb C., Aubin J., Poux M., 2023, Effect of Jet Nozzle Position on Mixing Time in Large Tanks. Processes, 11, 2200.
Patwardhan A.W., Gaikwad S.G., 2003, Mixing in Tanks Agitated by Jets. Chemical Engineering Research and Design, 81, 211–220.
Savarese M., Procacci A., Iavarone S., Giuntini L., Paepe W.D., Parente A., 2024, A sparse sensing and Chemical Reactor Network based framework for the development of physics-based digital twins of combustion devices. Proceedings of the Combustion Institute, 40, 105536.
Xu F., Sakurai K., Sato Y., Sakai Y., Sabu S., Kanayama H., Satou D., Kansha Y., 2023, Soft-Sensor Modeling of Temperature Variation in a Room under Cooling Conditions. Energies, 16, 2870.
Xu F., Wang J., Sakai Y., Sabu S., Kanayama H., Zhang R., Satou D., Kansha Y., 2025, Gray-box virtual sensor with constraints for predicting room temperature in cooling and heating modes. Building and Environment, 273, 112729.